Monitoring nonadiabatic avoided crossing dynamics in molecules by ultrafast X-ray diffraction

Markus Kowalewski,[1,a),b)] Kochise Bennett,[1,2,b)] and Shaul Mukamel[1,2,c)]

[1]*Chemistry Department, University of California, Irvine, California 92697-2025, USA*
[2]*Department of Physics and Astronomy, University of California, Irvine, California 92697-2025, USA*

We examine time-resolved X-ray diffraction from molecules in the gas phase which undergo nonadiabatic avoided-crossing dynamics involving strongly coupled electrons and nuclei. Several contributions to the signal are identified, representing (in decreasing strength) elastic scattering, contributions of the electronic coherences created by nonadiabatic couplings in the avoided crossing regime, and inelastic scattering. The former probes the charge density and delivers direct information on the evolving molecular geometry. The latter two contributions are weaker and carry spatial information through the transition charge densities (off-diagonal elements of the charge-density operator). Simulations are presented for the nonadiabatic harpooning process in the excited state of sodium fluoride. © *2017 Author(s). All article content, except where otherwise noted, is licensed under a Creative Commons Attribution (CC BY) license (http://creativecommons.org/licenses/by/4.0/).* [http://dx.doi.org/10.1063/1.4984241]

I. INTRODUCTION

X-ray diffraction[1–3] has been used for over a century to probe the structure of crystals and has been extended to diffuse scattering from liquids, probing nearest-neighbor distances, and serves as inspiration for the conceptually similar electron diffraction technique.[4,5] Time-resolved X-ray diffraction (TRXD) can track the structural changes that characterize phase transitions and chemical reactions and has been actively pursued to create movies of elementary molecular events.[5–18] Free electron lasers generate extremely bright and ultrafast X-ray pulses. That makes it possible to push diffraction to the single-molecule limit,[19–24] eliminating the need for time-consuming crystal preparation. In addition, their femtosecond timescale opens up the possibility of tracking ultrafast electronic dynamics, while their brightness may permit even weak signals, such as inelastic scattering from transient electronic coherences, to be measured.[25–30]

In this paper, we show how TRXD may be used to obtain real-time stroboscopic snapshots of nonadiabatic molecular dynamics. Nonadiabatic processes control virtually all photochemical and photophysical processes in molecules. For a single active vibrational coordinate, this results in avoided crossings. With two or more vibrational degrees of freedom, conical intersections (CoIns) become possible. As a molecule passes through a conical intersection[31] or avoided crossing, a short-lived electronic coherence is created, which can be spectroscopically detected[32,33] by X-rays. Examples for photochemical reactions that are mediated by a CoIn and have been studied by TRXD[34] are the ring-opening reaction in cyclohexadiene[35,36] and the cis/trans isomerization in the photoactive yellow protein.[37] Potential signatures in TRXD signals

a)Electronic mail: mkowalew@uci.edu
b)M.K. and K.B. contributed equally to this work.
c)Electronic mail: smukamel@uci.edu

    4, 054101-1

include measuring the geometric (Berry) phase,[38] which has so far eluded detection in molecules.

We examine the elastic and inelastic contributions to the diffraction pattern that stem from the coupled nonadiabatic electronic + nuclear dynamics in the vicinity of an avoided crossing. Time-resolved scattering from photoexcited molecules in the gas phase is given by an incoherent sum of single-molecule contributions. It therefore varies from the amplitude-squared form of the Bragg scatttering, containing elastic and inelastic terms, and may depend on electronic coherence.[39,40,42] We calculate the TRXD by an ensemble of molecules prepared in a superposition of valence electronic and vibrational states. We identify five basic contributions to the signal and study their relative intensity and time-resolved diffraction pattern. Contributions from electronic coherences, which are created in the avoided crossing region, are of particular interest and the underlying molecular quantities are the transition charge densities between electronic states. The nonadiabatic dynamics of sodium iodide has been investigated in Ref. [41], which did not address the signatures of electronic coherences. We examine the nonadiabatically coupled electronic + nuclear motions and the signatures of electronic coherences in the diffraction signal of a similar molecule, sodium fluoride.

II. THE INTERPLAY OF POPULATIONS AND COHERENCES IN SINGLE-MOLECULE DIFFRACTION OF NONADIABATIC DYNAMICS

Our study starts with the following expression for the off-resonant scattering signal in the gas phase (see Appendix A for derivation)

$$S(\mathbf{q}, t) = N \int dt |E_p(t)|^2 \langle \hat{\sigma}^\dagger(\mathbf{q}, t)\hat{\sigma}(\mathbf{q}, t) \rangle, \tag{1}$$

where $E_p(t)$ is the temporal envelope of the X-ray pulse, $\langle \ldots \rangle$ stands for the expectation value over the nuclear and electronic states, and $\hat{\sigma}(\mathbf{q}, t)$ is the spatial Fourier transform of the electronic charge-density operator and $\mathbf{q}$ is the scattering momentum transfer. Note that Eq. (1) comes with $\langle \hat{\sigma}^\dagger(\mathbf{q}, t)\hat{\sigma}(\mathbf{q}, t) \rangle$, while the classical equation for diffraction in crystals comes with $|\langle \hat{\sigma}(\mathbf{q}) \rangle|^2$.

The total charge-density operator for a system composed of molecules can be written as a sum of the charge densities from each molecule

$$\hat{\sigma}_{\mathrm{T}}(\mathbf{r}) = \sum_\alpha \hat{\sigma}_\alpha(\mathbf{r} - \mathbf{r}_\alpha) = \sum_\alpha \int d\mathbf{q} e^{i\mathbf{q}\cdot(\mathbf{r}-\mathbf{r}_\alpha)} \hat{\sigma}_\alpha(\mathbf{q}), \tag{2}$$

where $\mathbf{r}_\alpha$ is the center of molecule α. This representation is exact for a sufficiently dilute system such that the molecules have non-overlapping charge distributions, since each electron (the fundamental X-ray scatterer) can be rigorously assigned to a specific molecule. The elastic diffraction signal from a system initially in the ground state $|g\rangle$ is

$$S(\mathbf{q}) = |\sigma_{gg}(\mathbf{q})|^2, \tag{3}$$

where $\sigma_{gg}(\mathbf{q}) = \langle g|\hat{\sigma}(\mathbf{q})|g\rangle$ is the ground-state charge density in $\mathbf{q}$-space. For identical molecules, the charge-density matrix elements of each molecule only differ by the spatial phase factor associated with the location of the molecule and we may drop the subscript α on σ.

We now apply these results to a molecular model consisting of two electronic states e, g, and a single active nuclear coordinate R (Fig. 1). The time-dependent wavefunction of each molecule in the ensemble will be expanded in the adiabatic basis

$$|\Psi(R, t)\rangle = \sum_{i\in\{g,e\}} c_i(t)|\chi_i(R, t)\rangle \otimes |\phi_i\rangle, \tag{4}$$
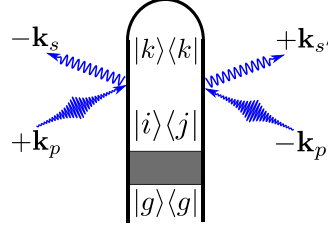
FIG. 1. Loop diagram for single-molecule X-ray scattering processes. The shaded area represents an excitation process that prepares the system in a superposition state by an actinic pump ($|g\rangle$ is the electronic ground state). We denote modes of the X-ray pulse with p and p', whereas s, s' represent relevant scattering modes ($\mathbf{k}_{p^{(\prime)}}$ has frequency $\omega_{p^{(\prime)}}$ and $\mathbf{k}_{s^{(\prime)}}$ has frequency $\omega_{s^{(\prime)}}$). For brevity we use $|\phi_i\rangle \rightarrow |i\rangle$ for the electronic states in this figure to aid readability. A complete set of diagrams for Eq. (6) is given in Fig. 2.

where $|\chi_i(R,t)\rangle$ is the (normalized) nuclear wave packet on the adiabatic electronic state $|\phi_i\rangle$ and $\sum_i |c_i|^2 = 1$ are the electronic state amplitudes. The time evolution of $|\Psi(R,t)\rangle$ is governed by the field-free nuclear Hamiltonian $\hat{H}_0$, which includes the nonadiabatic coupling matrix elements that account for CoIns or avoided crossings in the time evolution. The elements of the reduced electronic density matrix $\tilde{\rho}$ are given by $\tilde{\rho}_{ij}(t) = c_i^*(t)c_j(t)\langle\chi_i(t)|\chi_j(t)\rangle = \rho_{ij}\langle\chi_i(t)|\chi_j(t)\rangle$, which depends on the dephasing caused by the adiabatic nuclear wave packet overlap in states i and j. Expanding the time-dependent densities in the electronic states using the diagram in Fig. 1 results in

$$S(\mathbf{q},t) = N \int dt |E_P(t)|^2 \sum_{ijk} \rho_{ij}(t)\langle\chi_i(t)|\hat{\sigma}_{ik}^\dagger(\mathbf{q})\hat{\sigma}_{kj}(\mathbf{q})|\chi_j(t)\rangle. \tag{5}$$

Figure 2 gives the complete set of diagrams. For a two electronic state model, these result in the following five contributions to the signal:

$$\langle\hat{\sigma}^\dagger(\mathbf{q},t)\hat{\sigma}(\mathbf{q},t)\rangle = \left\{ \underbrace{\rho_{ee}(t)\langle\chi_e(t)|\hat{\sigma}_{ee}^\dagger\hat{\sigma}_{ee}|\chi_e(t)\rangle}_{(i)} + \underbrace{\rho_{gg}(t)\langle\chi_g(t)|\hat{\sigma}_{gg}^\dagger\hat{\sigma}_{gg}|\chi_g(t)\rangle}_{(ii)} \right.$$
$$+ \underbrace{\rho_{ee}(t)\langle\chi_e(t)|\hat{\sigma}_{eg}^\dagger\hat{\sigma}_{ge}|\chi_e(t)\rangle}_{(iii)} + \underbrace{\rho_{gg}(t)\langle\chi_g(t)|\hat{\sigma}_{ge}^\dagger\hat{\sigma}_{eg}|\chi_g(t)\rangle}_{(iv)}$$
$$\left. + \underbrace{2\Re\left[\rho_{eg}(t)\langle\chi_e(t)|\hat{\sigma}_{ee}^\dagger\hat{\sigma}_{eg}|\chi_g(t)\rangle + \rho_{eg}(t)\langle\chi_e(t)|\hat{\sigma}_{eg}^\dagger\hat{\sigma}_{gg}|\chi_g(t)\rangle\right]}_{(v)} \right\}, \tag{6}$$

where the electronic populations and coherences are given by the diagonal and off-diagonal elements of the density matrix $\rho_{ij}(t) \equiv c_i^*(t)c_j(t)$, respectively, and we have defined the electronic-state matrix elements of the charge-density operator $\hat{\sigma}_{ij} \equiv \langle\phi_i|\hat{\sigma}(\mathbf{q})|\phi_j\rangle$ (which remains an operator in the nuclear space and we omit the $\mathbf{q}$ dependence for brevity). Equation (6) agrees with earlier results[39,40] but identifies the different contributions in the adiabatic basis.

The first two terms on the right-hand side of Eq. (6) (i) and (ii) represent the elastic diffraction from states e and g, respectively, which encode the time evolution of the nuclear wave packets in the two electronic states. The next two terms, (iii) and (iv), represent the inelastic ($\sigma_{eg}^{(\dagger)}$) scattering from the electronic ground and excited state populations. The last term (v) is due to scattering off electronic coherences between $|g\rangle$ and $|e\rangle$.

Diffraction is often analyzed by assuming that the molecular electronic charge density is solely composed from the atomic densities. In case the molecule is in the electronic state e, Eq. (6) can be simplified by the independent atom approximation[15,43,44]
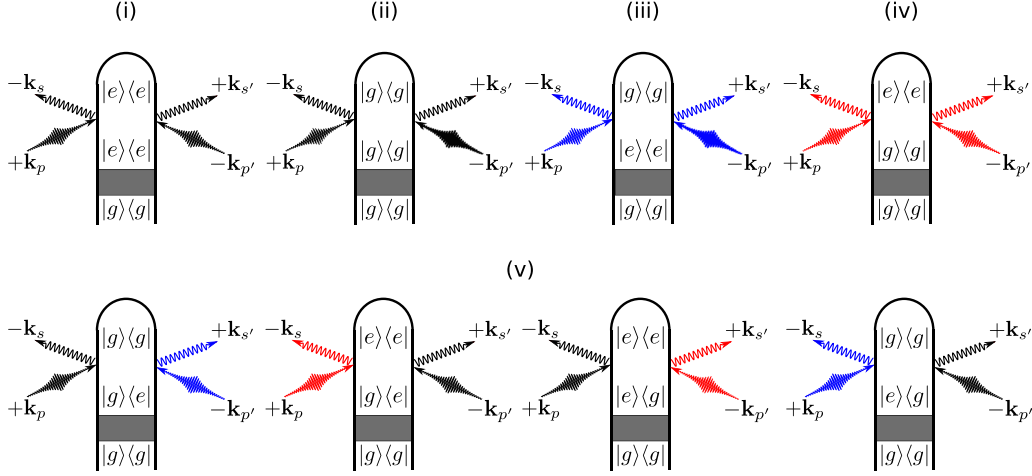
FIG. 2. Loop diagrams for single-molecule X-ray scattering processes as given by Eq. (5) and Fig. 4. The shaded area represents an arbitrary excitation that prepares the system in a superposition state of $|g\rangle$ and $|e\rangle$. Diagrams for elastic scattering from e and g are shown in (i) and (ii) respectively, while the diagrams for inelastic scattering from e and g are displayed in (iii) and (iv). The bottom row (v) represents all diagrams involving to electronic coherences. We denote modes of the X-ray probe pulse with p and p', whereas s, s' represent relevant scattering modes ($\mathbf{k}_{p^{(i)}}$ has frequency $\omega_{p^{(i)}}$ and $\mathbf{k}_{s^{(i)}}$ has frequency $\omega_{s^{(i)}}$). Elastic scattering processes come with $\hat{\sigma}_{gg}$ or $\hat{\sigma}_{ee}$ and are denoted by black field arrows. Inelastic processes in which the molecule gains (Stokes) or loses (anti-Stokes) energy to the field come with $\hat{\sigma}_{ge}$ or $\hat{\sigma}_{eg}$ depending whether the action is on the ket or bra and are denoted with red and blue field arrows to indicate the field's spectral shift due to the particular diagram. Note that we use $|i\rangle$ instead of $|\phi_i\rangle$ for the electronic states in this figure to aid readability.

$$\tilde{S}_{1,i.a.}(\mathbf{q}) = \sum_a \sum_{b<a} |f_a(\mathbf{q})||f_b(\mathbf{q})| \cos\left(\phi_b(\mathbf{q}) - \phi_a(\mathbf{q})\right)$$
$$\times \int d\mathbf{R} e^{i\mathbf{q}\mathbf{R}} \chi_e^*(\mathbf{R})\chi_e(\mathbf{R}), \tag{7}$$

where $f_a(\mathbf{q})$ is the atomic charge density of the ath atom in the molecule and $\phi_a(\mathbf{q})$ is its phase factor. This widely used expression approximates term (i) in Eq. (6) but does not account for inelastic scattering events and contributions due to electronic coherences. Our theory explicitly separates inelasticities, which are described by transition charge densities $\hat{\sigma}_{ij}(\mathbf{q})$ $(i \neq j)$ that interfere with ground and excited state terms $\hat{\sigma}_{ii}(\mathbf{q})$.

III. AVOIDED CROSSING DYNAMICS IN SODIUM FLUORIDE

We now present and discuss the five contributions to the diffraction signal from sodium fluoride. This molecule possesses a similar electronic structure to sodium iodide, the avoided crossing of which was studied in Zewail's landmark optical experiment.[45] Excited-state diffraction of sodium iodide has been calculated[41] by including the nonadiabatic dynamics but focusing solely on the elastic scattering processes [corresponding to terms (i) and (ii)]. An avoided crossing between the ionic and covalent states at 8 Å, known as harpooning, creates an electronic coherence in the course of the time evolution of the excited state nuclear wave packet (see Fig. 3). Iodine is a strong X-ray scatterer, and its large nuclear charge leads to a charge density distribution, which is heavily dominated by its core electrons. While this is still the case for molecular form factors of lighter element compounds, they have a more prominent contribution from valence electrons compared to the core electrons. The coherence contributions, which depend on the transition densities and are dominated by the rearrangement of valence electrons, are thus expected to be relatively stronger in sodium fluoride than in sodium iodide.

A. Electronic structure calculations and nonadiabatic wave packet dynamics

The electronic structure of NaF was calculated with the program package Molpro[46] at the CAS(8/9)/MRCI/aug-cc-pVTZ level of theory. A Douglas-Kroll-Hess 10th-order correction has
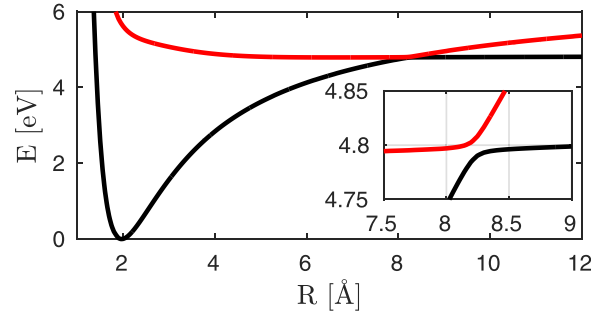
FIG. 3. Adiabatic potential energy surfaces for the electron harpooning in NaF (ionic state $X^1\Sigma\,|g\rangle$ black, covalent state $A^1\Sigma$, $|e\rangle$ red). The inset displays a close up of the avoided crossing region.

been used[47,48] to account for scalar relativistic effects caused by the core electrons. All densities were evaluated from the state specific charge density matrices (and transition charge density matrices) $P^{(ij)}$, expanded in the atomic orbital basis functions $\phi_s(\mathbf{r})$

$$\hat{\sigma}_{ij}(\mathbf{q};R) = \int d\mathbf{r}\, e^{-i\mathbf{q}\cdot\mathbf{r}} \sum_{rs} P^{(ij)}_{rs}(R)\phi_r^*(\mathbf{r};R)\phi_s(\mathbf{r};R). \qquad (8)$$

Both the transition dipole and the integrated transition density, $\int dr|\sigma_{ge}|$ shown in Fig. 4, peak at the avoided crossing point. The matrix elements of the electronic density operator $\hat{\sigma}_{ik}^*(\mathbf{q};R)\hat{\sigma}_{kj}(\mathbf{q};R)$ are displayed in Fig. 5. For clarity, we only show the projection along the direction of molecular axis obtained by integrating over the perpendicular directions. The diagonal density $\hat{\sigma}_{ee}^2$ [Fig. 5(a)] is clearly dominated by contributions from the core electrons, and the stripe pattern reflects the bond length in reciprocal space [see Eq. (1)]. The transition density $\hat{\sigma}_{ge}^2$ [Fig. 5(b)] mainly contains contributions from the valence orbitals involved in the transition. It is about 4 orders weaker than the diagonal matrix element [Fig. 5(a)]. However, it peaks at the avoided crossing, making it most suitable for the detection of inelastic contributions. The mixed matrix element $\hat{\sigma}_{ee}^\dagger\hat{\sigma}_{eg}$ [Fig. 5(c)] is a product of the electronic charge densities and the transition densities.
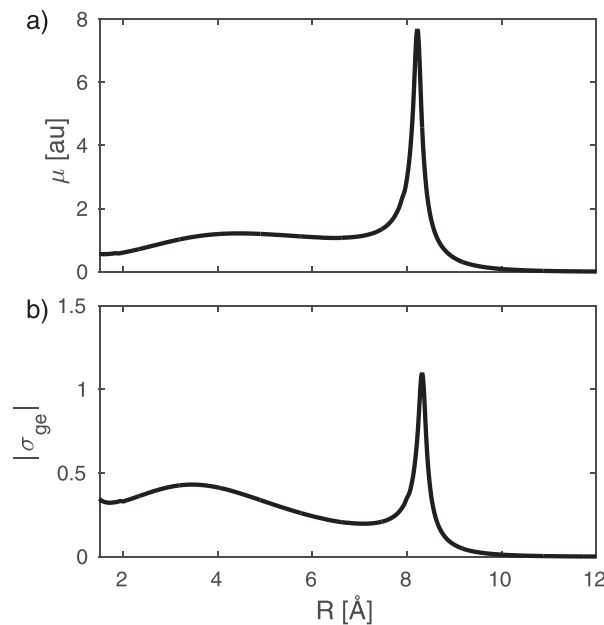

FIG. 4. Transition dipole moment μ_{ge} between the X and A states of NaF (a) and magnitude of the transition density σ_{ge} (b).
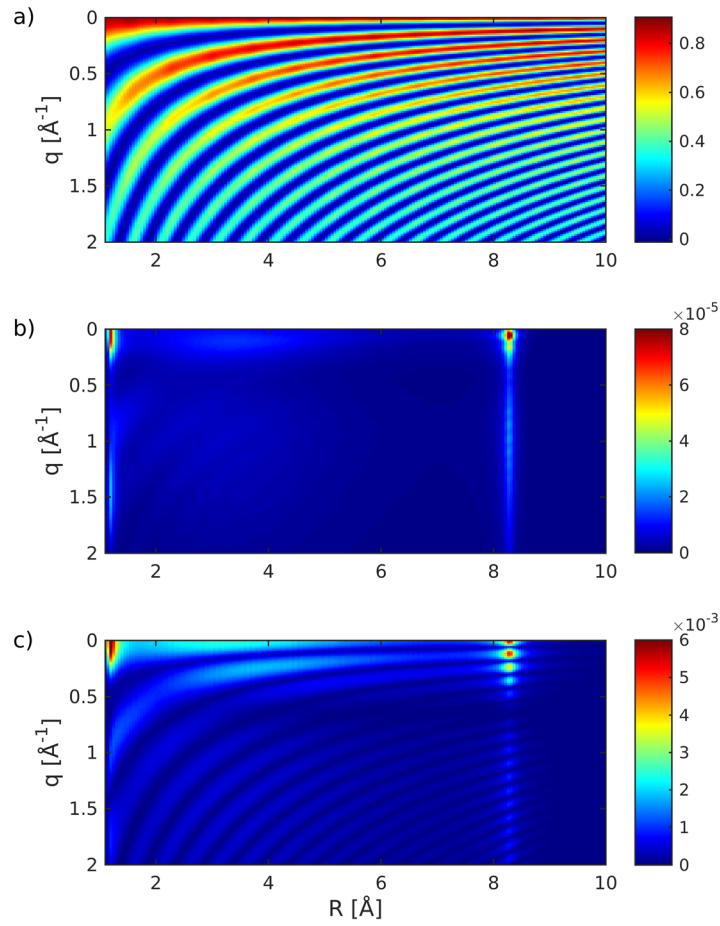
FIG. 5. Relevant density operator matrix elements in the nuclear subspace of NaF [obtained using Eq. (8)]: (a) $\hat{\sigma}^2_{ee}(\mathbf{q}, R)$, (b) $\hat{\sigma}^2_{ge}(\mathbf{q}, R)$, and (c) $|\hat{\sigma}^\dagger_{ee}(\mathbf{q}, R)\hat{\sigma}_{ge}(\mathbf{q}, R)|$. $\hat{\sigma}^2_{gg}$ is not shown due to its visual similarity to $\hat{\sigma}^2_{ee}$.

Nuclear wave packet dynamics simulations were carried out on a numerical grid with 1200 grid points for the nuclear coordinate R (extending from 2 to 24 Å) and the electronic states g and e. The Hamiltonian, which describes the coupled electronic and vibrational degrees of freedom, is given by

$$\hat{H} = \begin{pmatrix} \hat{T} + \hat{V}_g(R) & -E_{pu}(t)\hat{\mu}_{ge}(R) + \hat{K}_{ge} \\ -E_{pu}(t)\hat{\mu}_{eg}(R) - \hat{K}_{eg} & \hat{T} + \hat{V}_e(R) \end{pmatrix}, \tag{9}$$

where

$$\hat{T} = -\frac{1}{2m}\frac{\partial^2}{\partial R^2} \tag{10}$$

is the kinetic operator of the nuclei, m the reduced mass of the nuclei, and

$$\hat{K}_{ge} = \frac{1}{2m}\left(2f_{ge}\frac{\partial}{\partial R} + \frac{\partial}{\partial R}f_{ge}\right) \tag{11}$$

approximates the non-adiabatic couplings[31,35]

$$f_{ge} = \frac{f_0}{(R - R_0)^2 + s^2} \tag{12}$$

is the non-adiabatic coupling matrix element between g and e and has been obtained by a fit to values calculated with the DDR routine in MOLPRO.[46] The fitted parameters are $f_0 = 0.0387$, $R_0 = 8.222$, and $s = 0.0778$ (all values in atomic units).

We assume a Gaussian pump-pulse envelope

$$E_{pu}(t) = E_0 \cos(\omega t) \exp(-2 \ln(2) t^2 / w^2), \tag{13}$$

where w is the full width at half maximum of the intensity profile E_{pu}^2. The probe-pulse is not included in the propagation but is treated pertubatively and is then included in the final signal calculation [Eq. (1)]. The wave function $\Psi(R, t) = (c_g(t) \chi_g(R, t), c_e(t) \chi_e(R, t))^T$ is obtained by propagating the vibrational ground state of the $X^1\Sigma$ state with a Chebyshev scheme[49] using the Hamiltonian Eq. (9). The kinetic operator is modified with a perfectly matched layer[50] for g to avoid spurious reflections at the edges of the grid (22 Å). The signal is then obtained by evaluating Eqs. (3) and (5) and inserting the time-dependent wave functions and density operators ($\hat{\sigma}_{ik}^\dagger \hat{\sigma}_{kj}$, as shown in Fig. 5). We use the adiabatic basis, but the calculation is exact. The electronic coherence is obtained from the combined electronic-nuclear wave function and includes dephasing caused by the overlap of the nuclear wave packets and its decay

$$\tilde{\rho}_{eg} = c_e^*(t) c_g(t) \langle \chi_e | \chi_g \rangle. \tag{14}$$

This results in the decay and revival of the electronic coherence. The wave packet dynamics in the excited state potential ($\chi_e(R, t)$) is depicted in Fig. 6. It passes through the avoided crossing between 200 and 240 fs and reaches its outer turning point around 500 fs. The time-dependent excited state population alongside with the magnitude of the electronic coherence is shown in Fig. 7. The two relevant valence states (Fig. 3) are the $X^1\Sigma^+$ ground state and the $A^1\Sigma^+$ state (referred to as g and e in the following). A UV pump-pulse creates an excited-state population $\rho_{ee} \approx 30\%$, triggering the nuclear wave packet dynamics in states g and e that is subsequently probed with a 2.5 fs X-ray probe pulse. The time dependent excited-state population and the coherence are displayed in Fig. 7. At around 200 fs, the excited-state nuclear wavepacket first reaches the avoided crossing and returns to the crossing between 750 and 900 fs.
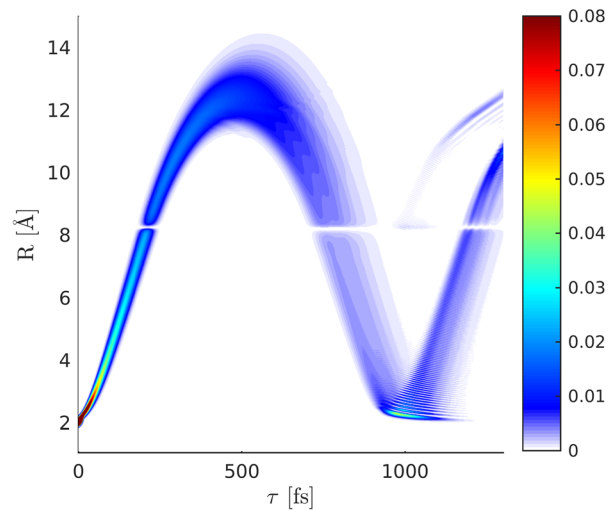

FIG. 6. Nuclear wave packet dynamics ($|\chi_e(R, t)|^2$) in the covalent $A^1\Sigma$ state following excitation with a 10 fs pump-pulse (FWHM).
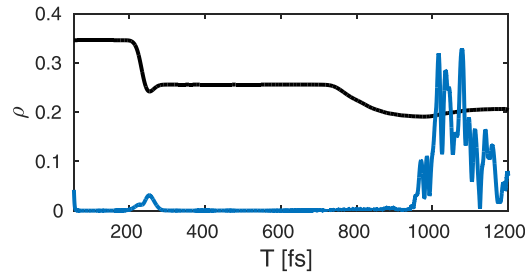
FIG. 7. Time evolution of the excited-state population ($A^1\Sigma$, black) and the magnitude of the coherence $|\rho_{eg}|$ (blue). The initial coherence created by the pump-pulse ($T < 50$ fs) is not shown. The coherence at 220 fs is created by the outward wave packet passing through the avoided crossing, while the strong coherence around 1100 fs corresponds to the wave packet return to the Franck-Condon region.

IV. THE DIFFRACTION SIGNAL

Figure 8 shows the diffraction pattern as well as the relative magnitude of the five contributions to the signal in Eqs. (6) and (1). The contributions to the diffraction signal are shown as labeled in Eq. (6) [(i) through (v), corresponding to the diagrams of Fig. 2]. The elastic diffraction signal, which stems from the charge density $\hat{\sigma}_{ee}$, is shown in Fig. 8(i). The time evolution represents the wave packet motion, i.e., the fringe spacing increases as the wave packet moves towards a longer bond length. The actinic pump-pulse (full width at half maximum 10 fs) also creates a non-stationary nuclear wave packet in the electronic ground state. This ground-state hole has a comparable magnitude to the excited state contribution Fig. 8(i). Figure 8(ii) shows the diffraction signal from the ground state density. The interference fringes are signatures of an oscillating vibrational wave packet in the ground-state potential. This hole burning phenomena will occur for pump-pulses that have bandwidths smaller than that of the Franck-Condon region.

The inelastic contribution that stems solely from the transition densities $\hat{\sigma}_{eg}$ and the excited-state wavepacket in Fig. 8(iii) is ≈ 4 orders of magnitude weaker. It carries no information about the electronic coherence but is dominated by the shape and magnitude of the transition density $\hat{\sigma}_{eg}^2$ and is closely related to the transition dipole moment. This contribution varies widely over time since the nuclear wavepacket enters a region where the transition dipole vanishes. The inelastic scattering from the ground state shown in Fig. 8(iv) is also modulated by the wavepacket motion. Compared to Fig. 8(iii), its intensity is only weakly modulated since it never reaches a region where the transition dipole moment vanishes.

Figure 8(v) depicts the combined contribution of inelastic scattering of the electronic coherences. This contribution is responsible for the time-evolving density caused by the electron dynamics.[42] At ≈ 220 fs, when the wavepacket hits the avoided crossing regime, an electronic coherence is created, resulting in a slow temporal oscillation that spreads over a wide range in q-space. This contribution is ≈ 3 orders of magnitude weaker than the excited-state density [Fig. 8(i)] but one order of magnitude larger than the other inelastic contributions (iii) and (iv). Another contribution appears at around 800 fs, which stems from the returning wavepacket, but it is much weaker due to the larger spread of the wavepacket. When the wavepacket returns to the Franck-Condon point, a larger spike in the coherence is visible in Fig. 7 at around 1100 fs. This contribution is averaged out in Fig. 8(v) due to the probe-pulse length and would require an attosecond rather than a femtosecond pulse to observe. Figure 9 shows the coherence contribution in Fig. 8(v) in real-space (Fourier transform). The first passage through the avoided crossing at 200 fs shows a clear signature at 8 Å, thus giving a hint of where the electronic coherence has been created. The second passage at around 800 fs is also visible.

V. CONCLUSIONS

In conclusion, the simulated gas-phase or single-molecule diffraction signal of sodium fluoride undergoing nonadiabatic avoided crossing dynamics contains signatures of the created
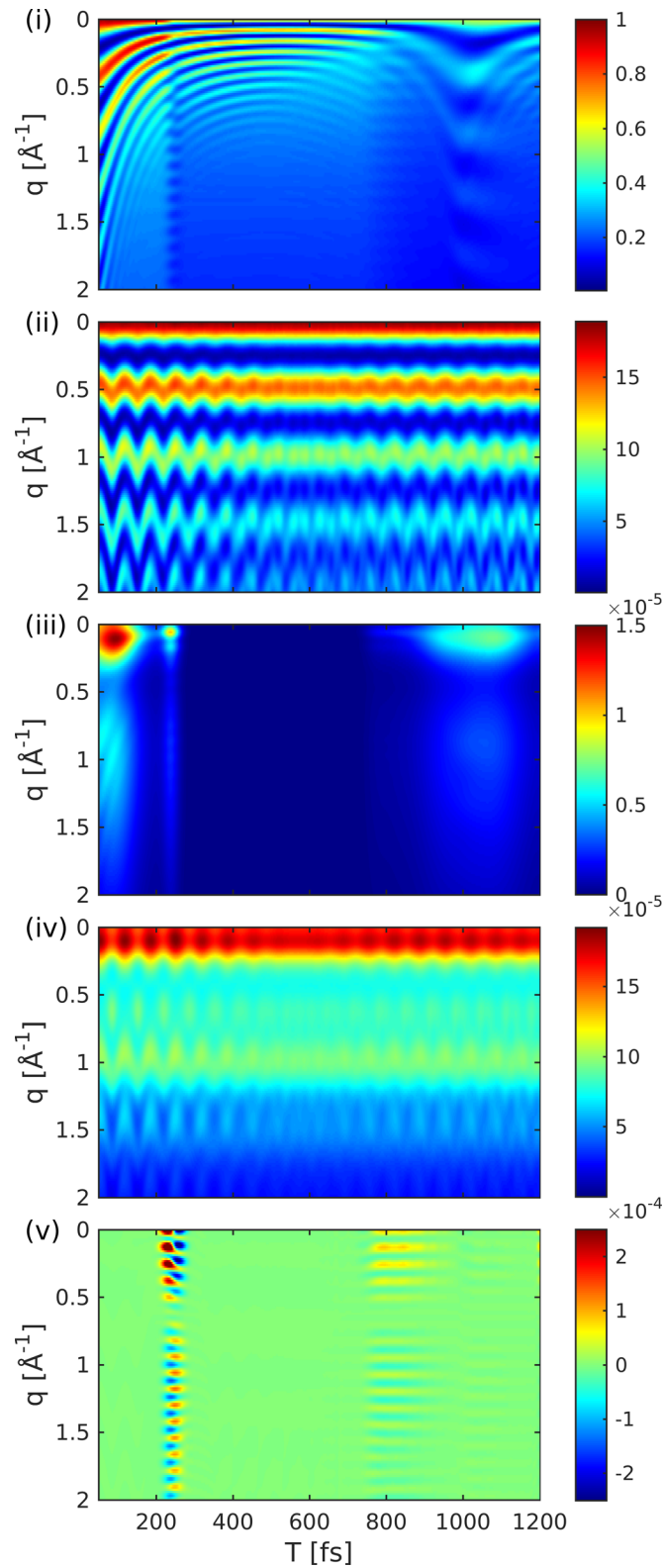
FIG. 8. Variation with a probe delay T of the five basic contributions to the gas-phase diffraction signal of NaF vs. the momentum transfer q. Panel labeling corresponds to Eq. (6). Signal intensities are normalized relative to (i). (i) and (ii) Elastic contributions from e and g, respectively. (iii) and (iv) Weaker inelastic contributions from e and g, respectively. (v) Combined contribution of inelastic scattering and electronic coherences whose intensity lies between the elastic and inelastic terms.
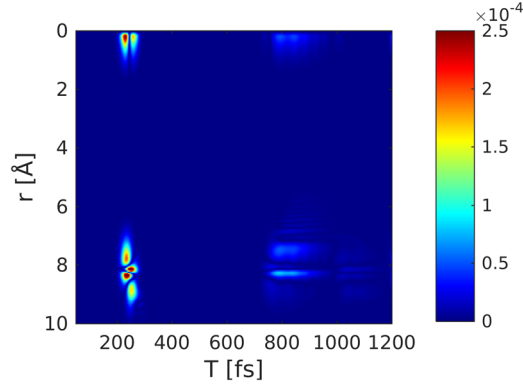
FIG. 9. Real-space picture of the coherence contribution to the TRXD signal obtained by a Fourier transform of Fig. 8(v).

electronic coherence on top of the dominant ground- and excited-state wavepacket motions. The diffraction signal depends on the ground- and the excited-state charge densities as well as the transition charge density that causes the inelastic contribution (v). These densities depend on time through the interatomic distance, which can be extracted directly from the diffraction signal. The shape of the nuclear wavepacket can be qualitatively retrieved without further phase reconstruction. For diatomic molecules, this allows to create a molecular movie out of the diffraction data. The coherence contributions do not merely indicate that a coherence has been created but also reveal where it has been created. Its contribution is significantly weaker than elastic scattering processes and appears as a rapid oscillation on top of the diffraction pattern. A recent XFEL diffraction study of molecular iodine in gas phase[17] claimed that the ground and excited state diffraction amplitudes interfere to form a holographic pattern. Our analysis does not support these claims.[18] It will be interesting to explore other nonlinear optical signals where the coherence contribution is more pronounced and possibly background-free.[32,33] Finally, we note that, by including additional nuclear coordinates, our approach may be used to predict signatures of CoIns in polyatomic molecules. Extended nonlinear probe schemes may be capable of directly imaging the transition density.

ACKNOWLEDGMENTS

APPENDIX A: THE SCATTERING SIGNAL

We start with the basic definition of the signal derived from the time-dependent perturbation theory, which allows its convenient dissection into its different contributions. In a previous work,[51] we derived the following expression for single-molecule frequency-resolved diffraction signals

$$S(\bar{\omega}, \mathbf{k}_s, \Lambda) = \int d\omega |\mathcal{F}_f(\omega, \bar{\omega})|^2 \omega'^2 \sum_\alpha \int d\omega_p d\omega_{p'} A_p(\omega_p) A_p^*(\omega_{p'}) e^{-i(\mathbf{q}-\mathbf{q}')\cdot\mathbf{r}_\alpha}$$
$$\times \langle \hat{\sigma}_\alpha(-\mathbf{q}', \omega_{p'} - \omega') \hat{\sigma}_\alpha(\mathbf{q}, \omega' - \omega_p) \rangle. \tag{A1}$$

In Eq. (A1), $A_p(\omega)$ is the vector potential envelope for the X-ray probe, $\mathcal{F}_f$ is a frequency gating (detector sensitivity) function, Λ stands for the set of parameters defining the X-ray field, and

$\mathbf{q}^{(\prime)} \equiv \frac{\omega}{c}\hat{\mathbf{k}}_s - \mathbf{k}_{p^{(\prime)}}$ is the momentum transfer ($\hat{\mathbf{k}}_s$ is the direction of the scattered wavevector). In standard applications, the molecules that compose the sample are assumed to have identical charge distributions and the subscripts α on the charge density should be dropped, as we will do for the remainder of this manuscript. Assuming no frequency resolution, we have $\mathcal{F}_f(\omega, \bar{\omega}) = 1$ for the frequency gating function. The long-range (inter-molecular) structure of the sample is captured by the structure factors

$$F_1(\mathbf{q}) = \sum_\alpha e^{-i\mathbf{q}\cdot\mathbf{r}_\alpha} \tag{A2}$$

in terms of which the diffraction signals can be written as

$$S_1(\mathbf{k}_s, \Lambda) = \int d\omega \frac{\omega^2}{\omega_p \omega_p'} \int d\omega_p d\omega_{p'} E_p(\omega_p) E_p^*(\omega_{p'})$$
$$\times F_1(\mathbf{q} - \mathbf{q}')\langle\hat{\sigma}(-\mathbf{q}', \omega_{p'} - \omega)\hat{\sigma}(\mathbf{q}, \omega - \omega_p)\rangle\rangle \tag{A3}$$

where we have substituted the electric field envelopes for the vector potential. For near-elastic scattering, we approximate $\frac{\omega}{\omega_p^{(\prime)}} \approx 1$, which is nearly valid even for inelasticities of several eV since the central frequency of the X-ray pulse is on the order of 10 keV. Similarly, the momentum transfer is approximated as independent of frequency. For the purpose of time-resolved diffraction studies, a time-domain expression is more convenient to simulate due to the nuclear motion. We thus substitute the time-domain charge density operator

$$\hat{\sigma}(\mathbf{q}, \omega) = \int dt\hat{\sigma}(\mathbf{q}, t)e^{i\omega t}, \tag{A4}$$

where we work in the interaction picture so that the operator time-dependence is through the field-free propagator, to obtain

$$S(\mathbf{q}, \Lambda) = F_1(0) \int d\omega \int dt dt' e^{i\omega(t-t')} E_p(t) E_p^*(t')\langle\hat{\sigma}(-\mathbf{q}, t')\hat{\sigma}(\mathbf{q}, t)\rangle, \tag{A5}$$

where we have replaced $\mathbf{k}_s$ by $\mathbf{q}$ in the argument in accordance with the quasi-elastic approximation. Upon carrying out the $d\omega$ integration and using $\hat{\sigma}(-\mathbf{q}) = \hat{\sigma}^*(\mathbf{q})$ finally results in Eq. (1)

APPENDIX B: THE ELECTRONIC CHARGE DENSITY OPERATOR

In this section, we discuss the operator nature of the charge density and its consequences. We will ignore nuclear dependence and will begin by considering a one-electron system. We seek an operator $\hat{\sigma}(\mathbf{r})$ such that the expectation value in a given state is the charge density

$$|\psi(\mathbf{r})|^2 \equiv \langle\psi|\hat{\sigma}(\mathbf{r})|\psi\rangle = \int d\mathbf{r}' d\mathbf{r}''\langle\psi|\mathbf{r}''\rangle\langle\mathbf{r}''|\hat{\sigma}(\mathbf{r})|\mathbf{r}'\rangle\langle\mathbf{r}'|\psi\rangle$$
$$= \int d\mathbf{r}' d\mathbf{r}''\psi^*(\mathbf{r}'')\psi(\mathbf{r}')\langle\mathbf{r}''|\hat{\sigma}(\mathbf{r})|\mathbf{r}'\rangle. \tag{B1}$$

This identifies the real-space matrix elements of the electronic charge density field operator

$$\sigma_{\mathbf{r}''\mathbf{r}'}(\mathbf{r}) \equiv \langle\mathbf{r}''|\hat{\sigma}(\mathbf{r})|\mathbf{r}'\rangle = \delta(\mathbf{r} - \mathbf{r}')\delta(\mathbf{r} - \mathbf{r}''). \tag{B2}$$

For a state decomposed into eigenmodes $|\psi\rangle = \sum_k c_i|i\rangle$, we have

$$\langle\psi|\hat{\sigma}(\mathbf{r})|\psi\rangle = \sum_{ij} \rho_{ij}\psi_i^*(\mathbf{r})\psi_j(\mathbf{r}), \tag{B3}$$

where $\rho_{ij} = c_i^* c_j$ are the electronic populations and coherences. Note that this matches the usual field-theoretic definition of the charge density $\hat{\sigma}(\mathbf{r}) = \hat{\psi}^\dagger(\mathbf{r})\hat{\psi}(\mathbf{r})$

1. The one-electron charge density operator of a many-electron system

We now extend the reasoning of the previous paragraph to an n-electron state $|\Psi\rangle$. The real-space identity operator in the space spanned by such states is

$$\int d\mathbf{r}_1 ... d\mathbf{r}_n |\mathbf{r}_1, ..., \mathbf{r}_n\rangle\langle\mathbf{r}_1, ..., \mathbf{r}_n| \equiv \int \{d\mathbf{r}\} |\{\mathbf{r}\}\rangle\langle\{\mathbf{r}\}| \tag{B4}$$

and the one-electron charge density is[52]

$$\int d\mathbf{r}_2 ... d\mathbf{r}_n |\Psi(\{\mathbf{r}\})|^2 = \langle\Psi|\hat{\sigma}(\mathbf{r})|\Psi\rangle$$

$$= \int \{d\mathbf{r}'\}\{d\mathbf{r}''\}\Psi^*(\{\mathbf{r}''\})\Psi(\{\mathbf{r}'\})\langle\{\mathbf{r}''|\hat{\sigma}(\mathbf{r})|\{\mathbf{r}'\}\rangle. \tag{B5}$$

Since the charge-density operator is a one-electron operator, we have the straightforward n-electron generalization of Eq. (B2)

$$\langle\{\mathbf{r}''|\hat{\sigma}(\mathbf{r})|\{\mathbf{r}'\}\rangle = \sum_m \delta(\mathbf{r} - \mathbf{r}_l')\delta(\mathbf{r} - \mathbf{r}_l'')\prod_{m\neq l}\delta(\mathbf{r}_m' - \mathbf{r}_m''), \tag{B6}$$

which is directly confirmed by substitution into Eq. (B5) and gives

$$\langle\Psi|\hat{\sigma}(\mathbf{r})|\Psi\rangle = \sum_{ij} \rho_{ij}\sigma_{ij}(\mathbf{r}), \tag{B7}$$

where we have identified

$$\sigma_{ij}(\mathbf{r}) = \int d\mathbf{r}_2 ... d\mathbf{r}_n \Psi_i^*(\mathbf{r}_1, ...\mathbf{r}_n)\Psi_j(\mathbf{r}_1, ...\mathbf{r}_n). \tag{B8}$$

We note that this result can equally well be obtained by the use of real-space field operators for many-electron systems as explicated by Cederbaum.[53,54] Moreover, Eq. (B8) is readily generalized to account for nuclear degrees of freedom $\mathbf{R}$ as

$$\hat{\sigma}_{ij}(\mathbf{r}) = \int d\mathbf{r}_2 ... d\mathbf{r}_n \Psi_i^*(\mathbf{R}, \mathbf{r}_1, ...\mathbf{r}_n)\Psi_j(\mathbf{R}, \mathbf{r}_1, ...\mathbf{r}_n), \tag{B9}$$

where the circumflex indicates that the left hand side remains an operator in the nuclear subspace due to dependence on $\mathbf{R}$.

[1]A. Guinier, *X-Ray Diffraction: In Crystals, Imperfect Crystals, and Amorphous Bodies* (Courier Dover Publications, 1994).
[2]J. Als-Nielsen and D. McMorrow, in *Elements of Modern X-ray Physics* (Wiley, Hoboken, 2011).
[3]P. Thibault and V. Elser, "X-ray diffraction microscopy," Annu. Rev. Condens. Matter Phys. **1**, 237–255 (2010).
[4]M. Ben-Nun, T. J. Martínez, P. M. Weber, and K. R. Wilson, "Direct imaging of excited electronic states using diffraction techniques: Theoretical considerations," Chem. Phys. Lett. **262**, 405–414 (1996).
[5]B. J. Siwick, J. R. Dwyer, R. E. Jordan, and R. D. Miller, "An atomic-level view of melting using femtosecond electron diffraction," Science **302**, 1382–1385 (2003).
[6]S. Bratos, F. Mirloup, R. Vuilleumier, and M. Wulff, "Time-resolved x-ray diffraction: Statistical theory and its application to the photo-physics of molecular iodine," J. Chem. Phys. **116**, 10615–10625 (2002).
[7]P. Coppens, I. I. Vorontsov, T. Graber, M. Gembicky, and A. Y. Kovalevsky, "The structure of short-lived excited states of molecular complexes by time-resolved x-ray diffraction," Acta Crystallogr., Sect. A: Found. Crystallogr. **61**, 162–172 (2005).
[8]H. Ihee, M. Lorenc, T. K. Kim, Q. Y. Kong, M. Cammarata, J. H. Lee, S. Bratos, and M. Wulff, "Ultrafast x-ray diffraction of transient molecular structures in solution," Science **309**, 1223–1227 (2005).

[9]M. Wulff, S. Bratos, A. Plech, R. Vuilleumier, M. Mirloup, M. Lorenc, Q. Kong, and H. Ihee, "Recombination of photo-dissociated iodine: A time-resolved x-ray-diffraction study," J. Chem. Phys. **124**, 034501 (2006).

[10]M. Cammarata, M. Levantino, F. Schotte, P. A. Anfinrud, F. Ewald, J. Choi, A. Cupane, M. Wulff, and H. Ihee, "Tracking the structural dynamics of proteins in solution using time-resolved wide-angle x-ray scattering," Nat. Methods **5**, 881–886 (2008).

[11]C. W. Siders, A. Cavalleri, K. Sokolowski-Tinten, C. Tóth, T. Guo, M. Kammler, M. H. V. Hoegen, K. R. Wilson, D. V. D. Linde, and C. P. J. Barty, "Detection of nonthermal melting by ultrafast X-ray diffraction," Science **286**, 1340–1342 (1999).

[12]M. Woerner, F. Zamponi, Z. Ansari, J. Dreyer, B. Freyer, M. Prémont-Schwarz, and T. Elsaesser, "Concerted electron and proton transfer in ionic crystals mapped by femtosecond x-ray powder diffraction," J. Chem. Phys. **133**, 064509 (2010).

[13]P. Coppens, "Molecular excited-state structure by time-resolved pump-probe x-ray diffraction. What is new and what are the prospects for further progress?," J. Phys. Chem. Lett. **2**, 616–621 (2011).

[14]R. Neutze and K. Moffat, "Time-resolved structural studies at synchrotrons and x-ray free electron lasers: Opportunities and challenges," Curr. Opin. Struct. Biol. **22**, 651–659 (2012).

[15]J. Yang, M. Guehr, X. Shen, R. Li, T. Vecchione, R. Coffee, J. Corbett, A. Fry, N. Hartmann, C. Hast *et al.*, "Diffractive imaging of coherent nuclear motion in isolated molecules," Phys. Rev. Lett. **117**, 153002 (2016).

[16]J. Larsson, R. W. Falcone *et al.*, "Ultrafast structural changes measured by time-resolved X-ray diffraction," Appl. Phys. A: Mater. Sci. Process. **66**, 587–591 (1998).

[17]J. Glownia, A. Natan, J. Cryan, R. Hartsock, M. Kozina, M. Minitti, S. Nelson, J. Robinson, T. Sato, T. van Driel *et al.*, "Self-referenced coherent diffraction x-ray movie of ångstrom-and femtosecond-scale atomic motion," Phys. Rev. Lett. **117**, 153003 (2016).

[18]M. K. Kochise Bennett and S. Mukamel, "Comment on 'self-referenced coherent diffraction x-ray movie of ångstrom-and femtosecond-scale atomic motion'," arXiv:1703.10113v1 (2017).

[19]R. C. Stevens, "High-throughput protein crystallization," Curr. Opin. Struct. Biol. **10**, 558–563 (2000).

[20]A. McPherson, *Crystallization of Biological Macromolecules* (Cold Spring Harbor Laboratory Press, 1999).

[21]J. Hajdu, "Single-molecule X-ray diffraction," Curr. Opin. Struct. Biol. **10**, 569–573 (2000).

[22]H. N. Chapman, "X-ray imaging beyond the limits," Nat. Mater. **8**, 299–301 (2009).

[23]D. Starodub, A. Aquila, S. Bajt, M. Barthelmess, A. Barty, C. Bostedt, J. Bozek, N. Coppola, R. Doak, S. Epp *et al.*, "Single-particle structure determination by correlations of snapshot X-ray diffraction patterns," Nat. Commun. **3**, 1276 (2012).

[24]S. Kahra, G. Leschhorn, M. Kowalewski, A. Schiffrin, E. Bothschafter, W. Fuß, R. de Vivie-Riedle, R. Ernstorfer, F. Krausz, R. Kienberger, and T. Schaetz, "Controlled delivery of single molecules into ultra-short laser pulses, a molecular conveyor belt," Nat. Phys. **8**, 238–242 (2012).

[25]M. Altarelli *et al.*, "The european X-ray free-electron laser," Technical Design Report No. DESY **97**, 2006.

[26]J. Feldhaus, J. Arthur, and J. B. Hastings, "X-ray free-electron lasers," J. Phys. B: At. Mol. Opt. Phys. **38**, S799 (2005).

[27]B. W. J. McNeil and N. R. Thompson, "X-ray free-electron lasers," Nat. Photonics **4**, 814–821 (2010).

[28]H. N. Chapman, P. Fromme, A. Barty, T. A. White, R. A. Kirian, A. Aquila, M. S. Hunter, J. Schulz, D. P. DePonte, and U. Weierstall, "Femtosecond X-ray protein nanocrystallography," Nature **470**, 73–77 (2011).

[29]C. Bostedt, J. Bozek, P. Bucksbaum, R. Coffee, J. Hastings, Z. Huang, R. Lee, S. Schorb, J. Corlett, P. Denes *et al.*, "Ultra-fast and ultra-intense x-ray sciences: First results from the linac coherent light source free-electron laser," J. Phys. B: At. Mol. Opt. Phys. **46**, 164003 (2013).

[30]A. Barty, J. Küpper, and H. N. Chapman, "Molecular imaging using x-ray free-electron lasers," Annu. Rev. Phys. Chem. **64**, 415–435 (2013).

[31]W. Domcke, D. R. Yarkony, and H. Köppel, *Conical Intersections* (World Scientific, 2011), Vol. 17.

[32]M. Kowalewski, K. Bennett, K. E. Dorfman, and S. Mukamel, "Catching conical intersections in the act: Monitoring transient electronic coherences by attosecond stimulated X-Ray raman signals," Phys. Rev. Lett. **115**, 193003+ (2015).

[33]M. Kowalewski, K. Bennett, J. R. Rouxel, and S. Mukamel, "Monitoring nonadiabatic electron-nuclear dynamics in molecules by attosecond streaking of photoelectrons," Phys. Rev. Lett. **117**, 043201+ (2016).

[34]M. P. Minitti, J. M. Budarz, A. Kirrander, J. S. Robinson, D. Ratner, T. J. Lane, D. Zhu, J. M. Glownia, M. Kozina, H. T. Lemke, M. Sikorski, Y. Feng, S. Nelson, K. Saita, B. Stankus, T. Northey, J. B. Hastings, and P. M. Weber, "Imaging molecular motion: Femtosecond X-Ray scattering of an electrocyclic chemical reaction," Phys. Rev. Lett. **114**, 255501 (2015).

[35]A. Hofmann and R. de Vivie-Riedle, "Adiabatic approach for ultrafast quantum dynamics mediated by simultaneously active conical intersections," Chem. Phys. Lett. **346**, 299–304 (2001).

[36]H. Tamura, S. Nanbu, T. Ishida, and H. Nakamura, "Ab initio nonadiabatic quantum dynamics of cyclohexadiene/hexatriene ultrafast photoisomerization," J. Chem. Phys. **124**, 084313+ (2006).

[37]K. Pande, C. D. M. Hutchison, G. Groenhof, A. Aquila, J. S. Robinson, J. Tenboer, S. Basu, S. Boutet, D. P. DePonte, M. Liang, T. A. White, N. A. Zatsepin, O. Yefanov, D. Morozov, D. Oberthuer, C. Gati, G. Subramanian, D. James, Y. Zhao, J. Koralek, J. Brayshaw, C. Kupitz, C. Conrad, S. Roy-Chowdhury, J. D. Coe, M. Metz, P. L. Xavier, T. D. Grant, J. E. Koglin, G. Ketawala, R. Fromme, V. Šrajer, R. Henning, J. C. H. Spence, A. Ourmazd, P. Schwander, U. Weierstall, M. Frank, P. Fromme, A. Barty, H. N. Chapman, K. Moffat, J. J. van Thor, and M. Schmidt, "Femtosecond structural dynamics drives the trans/cis isomerization in photoactive yellow protein," Science **352**, 725–729 (2016).

[38]D. Xiao, M.-C. Chang, and Q. Niu, "Berry phase effects on electronic properties," Rev. Mod. Phys. **82**, 1959–2007 (2010).

[39]J. Cao and K. R. Wilson, "Ultrafast x-ray diffraction theory," J. Phys. Chem. A **102**, 9523–9530 (1998).

[40]N. E. Henriksen and K. B. Møller, "On the theory of time-resolved x-ray diffraction," J. Phys. Chem. B **112**, 558–567 (2008).

[41]U. Lorenz, K. B. Møller, and N. E. Henriksen, New J. Phys. **12**, 113022+ (2010).

[42]G. Dixit, O. Vendrell, and R. Santra, "Imaging electronic quantum motion with light," Proc. Natl. Acad. Sci. U. S. A. **109**, 11636–11640 (2012).

[43]L. S. Bartell and R. M. Gavin, "Effects of electron correlation in X-Ray and electron diffraction," J. Am. Chem. Soc. **86**, 3493–3498 (1964).

[44]I. Waller and D. R. Hartree, "On the intensity of total scattering of X-Rays," Proc. R. Soc. A-Math. Phys. **124**, 119–142 (1929).

[45]T. S. Rose, M. J. Rosker, and A. H. Zewail, "Femtosecond real-time probing of reactions. IV. The reactions of alkali halides," J. Chem. Phys. **91**, 7415–7436 (1989).

[46]H.-J. Werner, P. J. Knowles, G. Knizia, F. R. Manby, and M. Schütz, See http://www.molpro.net for "MOLPRO, version 2015.1, a package of ab initio programs," (2015).

[47]M. Douglas and N. M. Kroll, "Quantum electrodynamical corrections to the fine structure of helium," Ann. Phys. N. Y. **82**, 89 (1974).

[48]B. A. Hess, "Relativistic electronic-structure calculations employing a two-component no-pair formalism with external-field projection operators," Phys. Rev. A **33**, 3742 (1986).

[49]H. T. Ezer and R. Kosloff, "An accurate and efficient scheme for propagating the time dependent schrödinger equation," J. Chem. Phys. **81**, 3967–3971 (1984).

[50]A. Nissen, H. O. Karlsson, and G. Kreiss, "A perfectly matched layer applied to a reactive scattering problem," J. Chem. Phys. **133**, 054306+ (2010).

[51]K. Bennett, J. D. Biggs, Y. Zhang, K. E. Dorfman, and S. Mukamel, "Time-, frequency-, and wavevector-resolved x-ray diffraction from single molecules," J. Chem. Phys. **140**, 204311 (2014).

[52]A. Szabo and N. S. Ostlund, *Modern Quantum Chemistry* (Dover Publications, New York, 1996).

[53]A. I. Kuleff and L. S. Cederbaum, "Radiation generated by the ultrafast migration of a positive charge following the ionization of a molecular system," Phys. Rev. Lett. **106**, 053001 (2011).

[54]L. S. Cederbaum, "Field operators in real space," J. Phys. Chem. A **120**, 3009–3014 (2016).